Materials Research Proceedings 41 (2024) 989-998 https://doi.org/10.21741/9781644903131-109

Formability analyses of AA6016-T4 aluminum alloy sheets subjected to roping

TVEIT Sigbjørn[1,a] and REYES Aase[1,b *]

[1]Department of Built Environment, Oslo Metropolitan University, Postboks 4, St. Olavs plass, NO-0130 Oslo, Norway

[a]sigbjorn.tveit@oslomet.no, [b]aase.reyes@oslomet.no

Keywords: Aluminum Alloys, FEA Based FLD, Roping

Abstract. Due to its good formability characteristics, AA6xxx aluminum alloys have become popular as a light-weight alternative to steel for car bodywork components produced by stamping. In the design of forming operations, numerical simulations are often used, and accurate material models to describe plasticity and forming limits are important to successfully design optimized products and production processes to avoid the reliance on trial and error. For aluminum alloys used in sheet metal forming, the anisotropic plasticity characteristics caused by the directional rolling process has therefore been subject to extensive research over the last decades. A previous experimental program on AA6016-T4 sheets showed that the formability of the material is strongly affected by roping caused by rolling. In this paper, models of anisotropic plasticity, isotropic hardening, instability, and fracture, along with an approach to describe the effects of roping for proportional strain paths are used to predict forming and fracture limits in LS-DYNA.

Introduction

The forming limit diagram (FLD) displays which strain combinations lead to strain localizations and which do not. Similarly, it is possible to construct fracture limit curves, which shows the strain combinations at fracture. In the traditional FLD, proportional straining is assumed through the full deformation process, but the influence of non-proportional straining can be studied for two-stage strain paths where formability tests are preceded by pre-strain. Graf and Hosford [1, 2] found that a biaxial pre-strain generally lowers the forming limits, while pre-straining by uniaxial tension can increase the forming limits. However, after pre-straining, the amount of possible additional plane-strain deformation depends on the effective strain during the pre-straining regardless of strain-path. In a previous study [3, 4], formability experiments were carried out for as-received and pre-strained sheets to investigate the effects of pre-strain by rolling on the formability of AA6016 sheets in the biaxial stretching region. In these tests, a significant anisotropy in forming limit strains were uncovered, and attributed to the roping phenomenon.

Roping (also called ridging) manifests itself as a directional surface defect that can appear in many aluminum alloys, copper alloys, and stainless steels at small strains [5-10]. It can be characterized by visible lines of up to hundreds of millimeters long along the rolling direction (RD), and a few millimeters apart in the transverse direction (TD) with a height difference between ridges and valleys of about 10-30 μm when the sheet is tensioned in TD [6, 8]. It impedes the use of these alloys in visible parts of e.g. vehicles due to aesthetics, but can also affect the formability [8] (as it can serve as a stress concentration) and bending properties of the materials [5]. Early studies analyzed the development of surface roughness and found that the amount of surface roughness is proportional to the through-thickness strain, and it has a linear dependence on the grain size [5].

The origin of roping in the aluminum alloy has been believed to intimately connect to texture distribution [6], and therefore, several studies are concentrated on the effect of the microstructure on roping [8, 9]. Jin studied how to reduce roping with the break-up of texture alignment [11].

More recently, some authors have studied the effects further. Muhammad et al. [5] studied the effects of roping (among others) on the bendability of aluminum alloys. They used crystal plasticity finite element model (CPFEM) and synthetic crystallographic textures to further investigate the relationship between through thickness clustering of similarly oriented grains, microstructure, and the observed surface topographic behavior. Hu et al. [6] introduced a roping index in the evaluation of the surface morphology and textures of four AA6XXX aluminum alloy sheets subjected to uniaxial tension. The same authors continued their investigation and applied CPFEM and developed an artificial neural network-based (ANN) model to predict thickness strain and corresponding surface roping under tensile deformation [7].

While several attempts to understand and describe the occurrence of the roping phenomenon in aluminum sheets based on crystal plasticity, less attention has been directed towards modelling the phenomenological effects of roping on forming limits and crack orientations. In this paper, based on the work of a master thesis [12], as a simple engineering approach, numerical forming and fracture limit diagrams are generated. Here, the roping is modeled by introducing perturbations to the sheet thickness based on the spatial distribution of effective plastic strains observed from experiments, and anisotropic plasticity, isotropic hardening, instability, and fracture are included in the finite element simulations in LS-DYNA.

Material and experimental details

The material assessed in this paper is AA6016 aluminum alloy, from virgin sheets of 1.5 mm thickness. Due to its good forming properties the rolled alloy is suited for use in the bodywork of cars. The metal sheets, produced by Hydro Aluminum Rolled Products GmbH, were rolled to their nominal thickness and solution heat treated before they were stored for six months natural aging process, giving them the temper designation T4. After heat treatment and natural ageing, the pre-strain was applied by cold rolling. All information regarding the characteristics of the sheets can be found in [4]. To characterize the material's anisotropic behavior, uniaxial tensile tests were carried out in seven different directions, and disc compression and plane strain tests were also performed. In the same study [4], the formability of the material was investigated by means of Marciniak tests [13], that were performed in a BUP600 forming machine using a flat punch with a diameter of 100 mm. The width of the samples was varied between 155 and 205 mm to attain different strain paths. Because of the material's anticipated anisotropic behavior, both samples oriented parallel and normal to the rolling direction were employed. In total, seven different strain paths were tested. After the experiments, one could clearly see some sort of irregularities on the surface of the specimens. This rough surface appeared like small ridges, all oriented in the same direction (Fig. 1) and could be identified as the roping phenomenon. The forming limit strains experienced a greater anisotropy than expected, an effect attributed to the severe roping [3].

Material models and determination of material parameters

In the present work, the numerical forming and fracture limit diagrams were generated by means of LS-DYNA [14], where *MAT_135 , also known as *MAT_WTM_STM [15] was employed. This is an elasto-viscoplastic constitutive model with an anisotropic yield criterion YLD2003 [16], the associated flow rule, non-linear isotropic work hardening rule (Voce), as well as a through-thickness instability criterion (TTSIC), and the Original Cockroft Latham Fracture Criterion (OCLFC). A Non-Local Extremal Thickness Strain Deviation Criterion (NLETSDC) was established to detect the onset of local necking from the available history variables.

Yield criterion: The Yld2003 yield criterion was proposed by Aretz [16] and contains eight anisotropy parameters that can be fitted to experimental data. The mathematical form can be found in the original work. There, the eight parameters are found from flow-stress ratios, $r_{\theta,}$ and transverse strain ratios, $R_{\theta,}$ from uniaxial tensile tests with longitudinal direction inclined at $\theta =$

Materials Research Proceedings 41 (2024) 989-998 https://doi.org/10.21741/9781644903131-109

0°, 45° and 90° to the sheet's rolling direction and the corresponding quantities taken from the equibiaxial flow stress and transverse strain ratios, r_b and R_b, respectively. LS-DYNA offers a direct calibration from these experimental data points, and these were found from the tensile and compression tests in [4], except for r_b which was taken as unity due to lack of experimental data. The eight data points used in the numerical analyses are given in Table 1, in addition to m, which is the non-quadratic yield function exponent.

Strain hardening: The strength of the material is defined by the flow stress, where the isotropic strain hardening is expressed by the extended Voce rule.

$$\sigma_e = \sigma_0 + Q_{R1}\left[1 - exp\left(-\mathrm{C}_{R1}\varepsilon_e^p\right)\right] + Q_{R2}\left[1 - exp\left(-\mathrm{C}_{R2}\varepsilon_e^p\right)\right] \quad (1)$$

Here, ε_e^p is the effective plastic strain, and Q_{Ri} and C_{Ri} are material constants. The equation was fitted to the experimental data from [4], and are given in Table 1.

The Non-Local Extremal Thickness Strains Deviation Criterion (NLETSDC): A simple non-local method was established to detect the onset of local necking from the available history variables in LS-DYNA. Initial geometric imperfections in terms of thickness variations are spatially distributed in the model, resulting in variable shell thicknesses among the different elements i. Within an area Ω_i around each element, the minimum and the maximum values of through-thickness plastic strains ε_z^p were monitored. From the relationship of the two quantities, a history variable was established as

$$\xi_i = \frac{\varepsilon_z^{p,\Omega_{min}}}{\varepsilon_z^{p,\Omega_{max}}} \quad (2)$$

The onset of local necking was assumed to occur when the history variable ξ_i reaches a critical value, ξ_{cr}. Different critical values were tested and are shown in Table 1.

The Through-Thickness Shear Instability Criterion (TTSIC): This criterion was first introduced by Bressan and Williams [17]. The following equation to calculate the inclination, φ, from the critical plane based on plastic strain increments is used. Here, the established coordinate system of *x*, *y*, and *z* is respectively aligned with the rolling, transverse, and through-thickness directions:

$$\cos 2\varphi = -\frac{d\varepsilon_y^p}{d\varepsilon_y^p + 2d\varepsilon_x^p} \quad (3)$$

TTSIC is satisfied when the shear stress on the critical plane,τ_φ, reaches a critical value, τ_{cr}.

$$\tau_\varphi = \frac{\sin(2\varphi)}{2}\sigma_1 \geq \tau_{cr} \quad (4)$$

The through-thickness shear instability criterion was calibrated in a one-step inverse modelling procedure in an LS-DYNA analysis of a single element with dimensions 1.2 mm by 1.2 mm, and the data from the plane strain tests (PST) from [4]. Note that it was not possible to achieve perfect

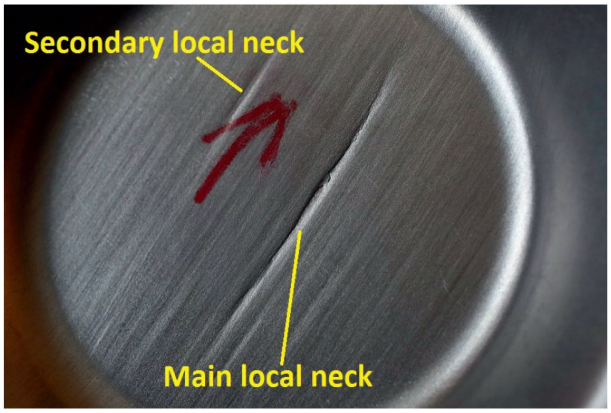

Fig. 1 Roping and multiple local necks observed at the bottom side of a Marciniak sample. Figure rendered from [4] with permission from the author.

*Table 1 Input to *MAT_135, taken or identified from the experimental data in [4].*

Strain hardening	Two-term Voce	σ_0	[MPa]	139.0
		Q_{R1}	[MPa]	44.26
		Q_{R2}	[MPa]	171.9
		C_{R1}	[-]	24.20
		C_{R2}	[-]	7.324
Yield criterion	Yld2003	r_0	[-]	1.000
		r_{45}	[-]	0.9986
		r_{90}	[-]	0.9910
		r_b	[-]	1.000
		R_0	[-]	0.6880
		R_{45}	[-]	0.4250
		R_{90}	[-]	1.030
		R_b	[-]	0.7850
		m	[-]	8
Instability criteria	NLETSDC	ξ_{cr}	[-]	1.5, 2.0, 3.0
	TTSIC	τ_{cr}	[MPa]	179.8
Fracture criteria	OCLFC	W_{cr}	[MPa]	211.5

plane strain in the tests [4], however, the strains in the x- and y- direction were measured by Digital Image Correlation (DIC) and the data can therefore be used for calibration. As the major strain direction in the plane strain tests (PST) is in the sheet's rolling direction, the principal axis of stress coincides with the principal axis of anisotropy. Thus, the angle of the inclination of the maximum shear plane, φ, can be calculated for an isotropic material. With fracture strains for the tests at $\bar{\varepsilon}^*_{x,PST} = 0.6237$ and $\bar{\varepsilon}^*_{y,PST} = -0.1323$, the inclination of the maximum shear plane, $\varphi = 48.41°$. A non-local proportional strain corresponding to the average strain path of the six PST tests from [4] was applied to the element, and when the FE analysis reached the average fracture strains from the experimental PST tests, the value of the major stress component $\sigma_1^* = \sigma_x^*$ was recorded. From this, the critical shear stress, τ_{cr}, was found as 179.8 MPa, and is given in Table 1.

The Original Cockcroft-Latham fracture criterion (OCLFC): This ductile fracture criterion is assumed to be satisfied when the accumulation of principal tensile stresses over the plastic deformation reaches a critical value, and is formulated as [18]

Materials Research Proceedings 41 (2024) 989-998 https://doi.org/10.21741/9781644903131-109

$$W_1 = \int_0^{\overline{\varepsilon^p}} \max(\sigma_1, 0) d\overline{\varepsilon^p} \geq W_{cr} \quad (5)$$

where $\overline{\varepsilon^p}$ is the accumulated plastic strain, and W_{cr} is a material constant which can be adjusted to observations from experiments where strain localization is controlled. In [4], two different plane strain tension tests specimen geometries with three parallels each were used to calculate the OCLFC. Averaging over the path, the critical plastic work was found as 211.5 MPa [4], and is also given in Table 1.

Modeling of roping

Aiming to model the effects of roping as scaled harmonic perturbations to the sheet thickness, a sum of four sine waves can be fitted to a sheet's thickness profile obtained from measurements. As the real thickness profile was not available from [4], a fictive thickness profile based on the mean thickness and standard deviations of the sheets sampled in the experimental program was used.

In LS-DYNA, a pre-programmed module to model perturbations to the thickness of shells as one or more harmonic waves exists in the keyword *PERTURBATION. The keyword allows the user to specify the amplitude, wavelength, and periodic offset of waves though the variables AMPL, WL, and OFF, respectively. Thickness perturbations due to roping can be modelled to satisfying accuracy by adding multiple harmonic perturbations to approximate a measured thickness distribution with the formulation [15]:

$$p(x,y) = \sum_{i=1}^{n} \left(AMPL_i \left[sin\left(2\pi \frac{x+XOFF_i}{XWL_i}\right) + sin\left(2\pi \frac{y+YOFF_i}{YWL_i}\right) \right] \right) \quad (6)$$

As roping is reported to be the manifestation of the orientation of grain's spatial distribution in the sheets' through-thickness direction [19], the observed effects in terms of thickness perturbations are accompanied with variation in material characteristics. Thus, naive of information about this variation, the modelled thickness perturbation could be scaled to obtain good correlation between the anisotropy predicted by the FE-models and the experimental results. In the MK model [13], the fundamental assumption is that a band of the sheet is somehow weaker than the rest. This weakness could be material variations or thickness variations. Aretz [20] compared the use of thickness and material imperfections to trigger localized necking in the MK model, and concluded that the two approaches are equivalent for proportional strain paths. Due to simplicity, imperfections are often thought of and modelled as a reduction in the thickness of the material. The magnitude of the imperfection is typically calibrated to match experimental observations. In the same way, a larger thickness variation than what is physically observed can be justified to account for reduced stiffness from spatial variations in material characteristics for proportional strain paths.

Limited information was available from the experimental tests about the nature of the roping phenomenon of the aluminum sheets. Thus, the distance between valleys formed by roping was approximated by visual inspections on the effective strain map from DIC for the last image prior to fracture [4]. Using the sample which most clearly showed the localizations of strains, namely the sample labelled as MK160-90-2, (see Fig. 2 (a)), the approximated distance between roping valleys was roughly measured to be 12.5 mm. With the reported non-local logarithmic fracture strain at 0.2870 for the sample, the initial distance was calculated to be approximately 8.9 mm.

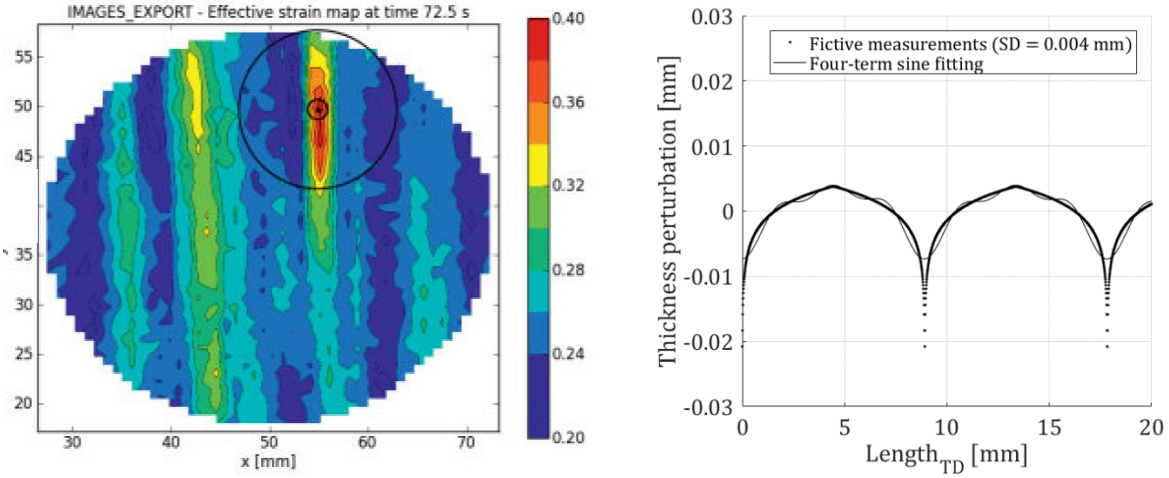

(a) (b)

Fig. 2 (a) Effective strain map at the last frame prior to fracture of the sample labelled as MK160-90-2 of virgin AA6016-T4 (ID=6), rendered from [4] with permission from the author. (b) Thickness perturbation along the length in the transverse direction.

Table 2 Fitted parameters of the four-term sine wave roping perturbation.

	$AMPL_i[mm]$	$YWL_i\ [mm]$	$YOFF_i\ [mm]$
i = 1	0.00168	4.462	3.382
i = 2	0.00130	2.976	-0.692
i = 3	0.00436	8.907	-2.267
i = 4	-5.2E-6	8.825	-5.549

From this estimated distance between grooves, along with the mean measured thickness of 1.496 mm and standard deviation of 0.004 mm from thickness measurements performed in the experimental study, a fictive thickness profile was established- The parameters of a four-term sine wave roping perturbation model was fitted to it, using the Sum of Sines Models-tool in MATLAB R2020a [20]. Fig. 2 (b) shows the fictive perturbation measurements along with the fitted four-term sine wave model, while Table 2 displays the amplitude, $AMPL_i$, wavelength, YWL_i, and off-set, $YOFF_i$, for each of the four harmonic functions, i.

With roping modelled as a four-term harmonic function in the transverse direction, no thickness variations are introduced in the sheet's rolling direction. In a perturbation plot generated from white-light interferometry images by Engler et al. [8], the valleys and ridges were accompanied by unstructured thickness deviations in the rolling directions. Attempting to simulate this, a FORTRAN-program which generated random unstructured thicknesses perturbations based on a mean thickness and a standard deviation, was used. As the random perturbation is added to the existing four-term sine wave perturbation, a rather moderate standard deviation of 0.002 mm was used along with the mean thickness of 1.496 mm. A scaling factor of six was used for the four-term sine wave perturbation. Fig. 3 (a) shows the thickness perturbation of the undeformed patch.

Formability and Fracture Diagrams with roping model

To construct the FEA-generated forming and fracture limit diagrams in LS-DYNA, a 60 mm by 60 mm squared patch of 50 by 50 Belytschko-Tsay shell elements was subjected to 15 different proportional biaxial deformations. The four individual edges were continuously constrained according to the illustration in Fig. 3 (b). A controlled displacement was then assigned to the right and the top edge in their normal directions to create the non-local, proportional, biaxial strain paths.

Along with the Yld2003 yield function, the NLETSDC, TTSIC, and OCLFC were used to predict local necking and/or fracture. Through the material keyword *MAT_135, TTSIC and OCLFC was employed as uncoupled criteria where satisfaction of either criterion in three out of the five through-thickness integration points in an element caused element erosion. As the

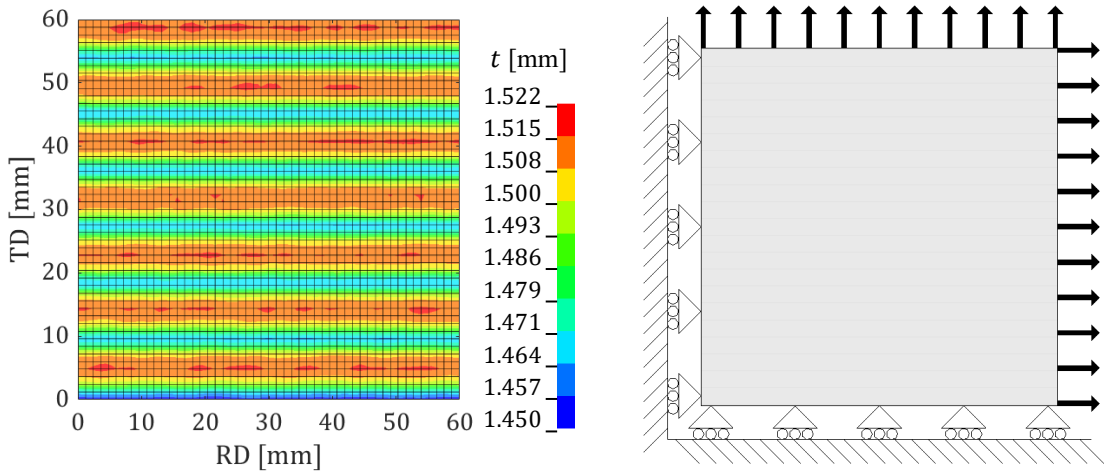

(a) (b)

Fig. 3 (a) Thickness variation of the FEA-model with four-term sine wave perturbation (Sc. = 6) and random perturbation with SD = 0.002 mm. (b) Boundary conditions of patch model subjected to biaxial strains paths for the construction of FEA-generated forming and fracture limit diagrams. The rolling supports should be considered continuous along the edges.

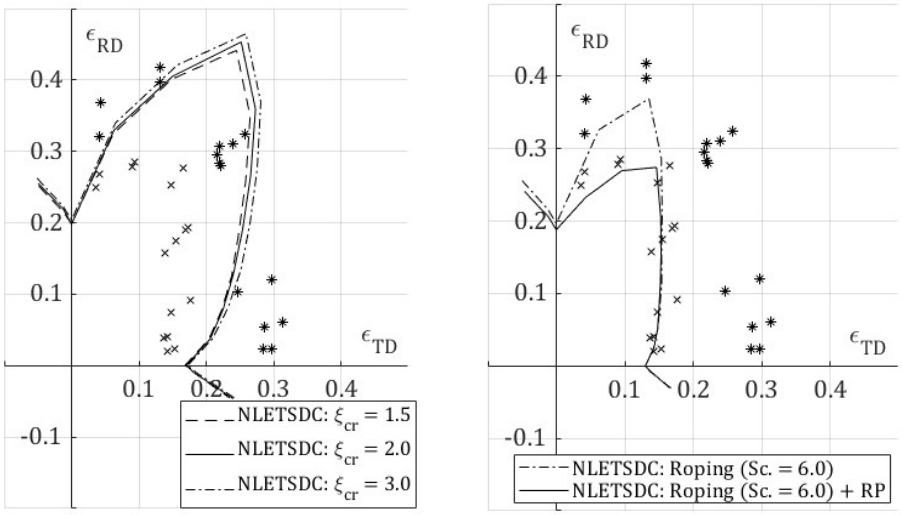

(a) (b)

Fig. 4 FLDs from NLETSDC for (a) different critical extremal thickness strain ratio and (b) with roping model scaled by a factor of six, with and without additional random thickness perturbation. The points are the experimental necking (crosses) and fracture (stars) strains from [4].

NLETSDC was not implemented in the material model, fulfillment of the criterion was manually monitored. When either criterion was satisfied, the displacements in the two directions were recorded, and the non-local strain values were calculated as the necking or fracture strains.

Materials Research Proceedings 41 (2024) 989-998 https://doi.org/10.21741/9781644903131-109

To test NLETSDC, a sensitivity analysis of the critical extremal thickness strain ratio, ξ_{cr} was carried out. On the model with unscaled roping perturbations and no random perturbation in the rolling direction , forming limit curves were plotted with the critical values set to 1.5, 2.0 and 3.0. The different curves, displayed in Fig. 4 (a), shows that variations in the critical value yields small differences in forming limits. For the further analyses, $\xi_{cr} =$ 2.0 was used as the critical value.With the four-term sine wave perturbation model unscaled (Sc. = 1.0), the forming limit diagram exhibited moderate anisotropy. The two plane strain configurations exhibited forming limits close to the measured values but were clearly overestimated as the strains approached biaxial symmetry.

Because roping is the manifestation of band clusters of grains with the same orientation, the material itself could be assumed to have varying material characteristics that are spatially distributed according to the sheet thickness. Thus, lacking information about this distribution of plasticity characteristics, a scaling of the four-wave sine perturbation was performed to simulate further reduced stiffness, to meet the strong anisotropy of forming limits observed in experiments for portional strain paths. The scaling was performed by multiplying the amplitude of each curve in the four-term sine wave model with a scalar ($Sc. = 2.0$ and 6.0) to amplify the effect of roping. From Fig. 5 (a), which displays the FLDs predicted by NLETSDC, it is evident that the effect of amplifying the roping perturbation model yielded significant reduction in forming limit strains in the sheet's transverse direction. With a scaling factor $Sc. = 6$, the predicted and measured results coincided very well for configurations where $\varepsilon_{TD} > \varepsilon_{RD}$. Nevertheless, the forming limit strains were still exaggerated by the FEA-model for its symmetric counterpart.

The FLDs with the roping model, with and without the random perturbation with standard deviation of 0.002 mm, are compared in Fig. 4 (b). When the harmonic perturbation was accompanied with the random perturbation, the forming limits for strain paths when $\varepsilon_{TD} > \varepsilon_{RD}$

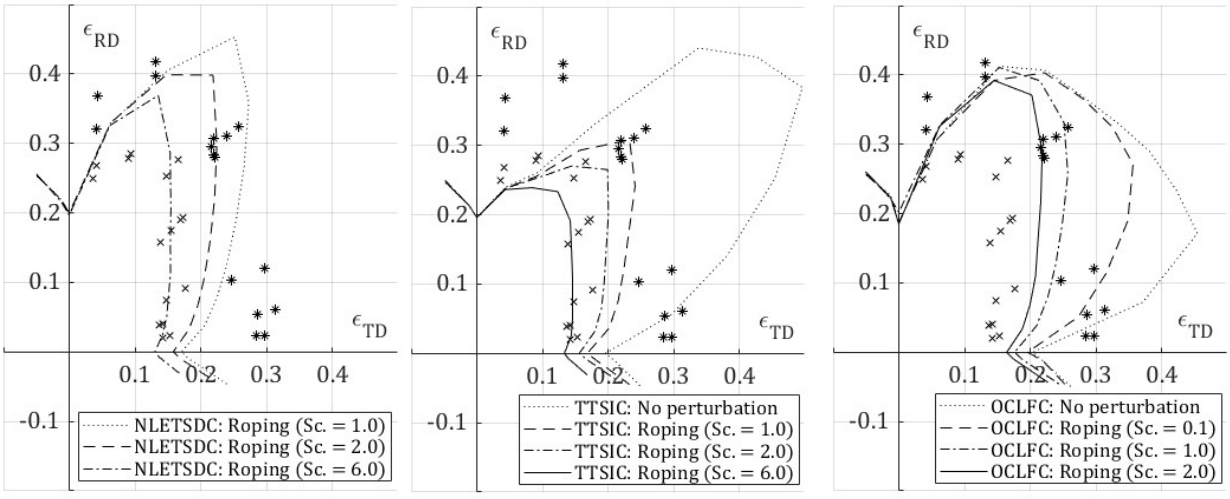

(a) (b) (c)

Fig. 5 Forming and fracture limit curves with and without the roping model, for different scales of the four-term sine wave perturbation for the (a) NLETSDC, (b) TTSIC, and (c) OCLFC. The points represent the experimental necking (crosses) and fracture (stars) strains from [4].

remained nearly unchanged, while its symmetric counterpart predicted drastically reduced necking strains, just on the conservative side of the experimentally detected forming limit strains.

Fig. 5 (b) and (c) displays the forming and fracture limit diagram generated for TTSIC and OCLFC, respectively, with different scaling factors to the harmonic perturbations. Evidently, the model with perfectly uniform thickness was not able to produce the shape nor the magnitude of

forming and fracture limits from experiments for neither criteria. However, with $Sc. = 6$, the TTSIC criterion can be said to predict conservative results compared to the experimental fracture strains, and the shape of the predicted fracture curveseems reasonable. For the OCLFC, $Sc. = 2$ was sufficient to obtain a reasonable shape for the fracture limit diagram and predict conservative results. Larger scale factors were therefore not tested for OCLFC The magnitudes of the predicted fracture strains were clearly underestimated for strain paths in vicinity to the two plane-strain axes,while strain paths near the equibiaxial axis displayed better agreement with the experimental data. Although the introduction of thickness perturbations helped, the OCLFC was not able to recreate the shape of the fracture strain curves in a satisfying way.

Conclusions

With the introduction of the harmonic thickness perturbations, together with the anisotropic yield criterion Yld2003, and the isotropic two-term Voce hardening law, experimental forming limits were recreated with good accuracy for proportional strain paths using one local necking instability criterion and two different fracture criteria. Without the introduction of the harmonic thickness petrurbations, all three criteria produced forming and fracture limits very different to what was observed in experiments. The best fit to experiments was achieved when the four-term sine wave perturbation, which was initially fitted to the amplitudes of measured thickness deviations, was scaled with a factor of six.

References

[1] A. Graf, W. Hosford, Effect of Changing Strain Paths on Forming Limit Diagrams of Al 2008-T4, Metall. Trans. A. 24 (1993) 2503-2512.

[2] A. Graf, W. Hosford, Influence of strain-path changes on forming limit diagrams of Al 6111 T4, Int. J. Mech. Sci. 36(10) (1994) 897-8910.

[3] D. Vysochinskiy, T. Coudert, O.S. Hopperstad, O.-G. Lademo, A. Reyes, Experimental study on the formability of AA6016 sheets pre-strained by rolling, Int. J. Mater. Forming. 11(4) (2018). 541-557. https://10.1007/s12289-017-1363-6

[4] D. Vysochinskiy, Formability of aluminium alloy subjected to prestrain by rolling, PhD Thesis, Department of Structural Engineering, Trondheim, Norwegian University of Science and Technology, 2014.

[5] W. Muhammad, U. Ali, A. P. Brahme, J. Kang, R. K. Mishra, K. Inal, Experimental analyses and numerical modeling of texture evolution and the development of surface roughness during bending of an extruded aluminum alloy using a multiscale modeling framework, Int. J. Plast. 117 (2019) 93-121. https://doi.org/10.1016/j.ijplas.2017.09.013

[6] Y. Hu, G. Zhou, R. Liu, X. Yuan, L. Cao, B. Yang, D. Li, P. Wu, On the correlation between roping, texture, and morphology of aluminium alloy sheets, J. Mater. Res. Technol. 26 (2023) 571-586. https://doi.org/10.1016/j.jmrt.2023.07.209

[7] Y. Hu, G. Zhou, X. Yuan, D. Li, L. Cao, W. Zhang, P. Wu, An artificial neural network-based model for roping prediction in aluminum alloy sheet, Acta Mater. 245 (2023) 118605. https://doi.org/10.1016/j.actamat.2022.118605

[8] O. Engler, C. Schäfer, H. J. Brinkman, Crystal-plasticity simulation of the correlation of microtexture and roping in AA 6xxx Al–Mg–Si sheet alloys for automotive applications, Acta Mater. 60(13–14) (2012) 5217-5232. http://dx.doi.org/10.1016/j.actamat.2012.06.039

[9] O. Engler, H. Moo-Young, C. N. Tome, Crystal-plasticity analysis of ridging in ferritic stainless steel sheets, Metall. Mater. Trans. A (Physical Metallurgy and Materials Science). 36A(11) (2005) 3127-3139.

[10] L. Qin, M. Seefeldt, P. Van Houtte, Analysis of roping of aluminum sheet materials based on the meso-scale moving window approach, Acta Mater. 84 (2015) 215-228. https://doi.org/10.1016/j.actamat.2014.10.054

[11] H. Jin, Breakup of texture alignment and reduction of roping in AA6111 aluminium alloy, Mater. Sci. Technol. 33(11) (2017) 1388-1396. https://doi.org/10.1080/02670836.2017.1295518

[12] S. Tveit, Formability analysis of AA6016-T4 aluminium alloy sheets subjected to roping, MSc Thesis, Department of Civil Engineering and Energy Technology, Oslo, Oslo Metropolitan University, 2020.

[13] Z. Marciniak, K. Kuczynski, Limit strains in the process of stretch-forming sheet metal, Int. J. Mech. Sci. 9 (1967) 600-620.

[14] J. O. Hallquist, Theoretical Manual, Livermore Software Technology Corporation, Livermore, California, 1998.

[15] LS-DYNA Keyword User's Manual. Volume II Material Models, Version 971 R6.1.0, Livermore Software Technology Corporation, Livermore, California, 2012.

[16] H. Aretz, Applications of a new plane stress yield function to orthotropic steel and aluminium sheet metals, Modelling Simul. Mater. Sci. Eng. 12 (2004) 491-509.

[17] J. D. Bressan, J. A. Williams, The use of a shear instability criterion to predict local necking in sheet metal deformation, Int. J. Mech. Sci. 25(3) (1983) 155-168.

[18] M. G. Cockcroft, D. J. Latham, Ductility and the Workability of Metals, Journal of the institute of metals. 96 (1968) 33-39.

[19] P. D. Wu, D. J. Lloyd, Analysis of surface roughening in AA6111 automotive sheet, Acta Mater. 52(7) (2004) 1785-1798. https://doi.org/10.1016/j.actamat.2003.12.039

[20] H. Aretz, A comparison between geometrical and material imperfections in localized necking prediction, in: E. Cueto, F. Chinesta (Ed.), Proc. 10th ESAFORM Conference on Material Forming, AIP Conference Proceedings, 2007, pp. 287-292.

[21] MATLAB & Simulink, Sum of Sine Models - R2020a, MathWorks Nordic, [Online]. Read on https://se.mathworks.com/help/curvefit/sum-of-sine.html the 7th April 2020